

Cumulus Clouds and Reflected Sunlight from Landsat ETM+

*G. Wen and L. Oreopoulos
National Aeronautics and Space Administration
Goddard Space Flight Center
University of Maryland Baltimore County
Joint Center of Earth System Technology
Greenbelt, Maryland*

*R. F. Cahalan and S. C. Tsay
National Aeronautics and Space Administration
Goddard Space Flight Center
Greenbelt, Maryland*

Introduction

Cumulus clouds attenuate solar radiation casting shadows on the ground. Cumulus clouds can also enhance solar radiation in the clear region nearby. The enhancement of down-welling solar radiation has been observed at the ground level in the clear region near cumulus clouds (Mims and Frederick 1994). The additional diffuse radiation source from cumulus clouds makes the clear gaps appear to be brighter from the space. If this effect is not accounted for, large errors may be introduced in aerosol optical thickness retrieval in the clear gaps in cumulus cloud field.

With 30 m resolution, the Landsat 7 Enhanced Thematic Mapper Plus (ETM+) instrument can resolve the clear gaps in fair weather cumulus cloud fields, allowing us to study the impact of cloud on clear-sky radiative transfer. In this study, we demonstrate that such effect can be observed from the high-resolution satellite instrument, and further be parameterized.

Data Description

The ETM+ on Landsat 7 has visible (bands 1, 2, and 3), near infrared (IR) (band 4), and mid-IR (bands 5 and 7) bands at 30-m spatial resolution, and a thermal IR band at 11 μm with 60-m resolution (band 6). In addition, the ETM+ has a panchromatic band with spatial resolution of 15-m. The improved ETM+ instrument has the ability to switch between high and low gain settings. The thermal band has both high and low gain settings operating at the same time.

A Landsat 7 ETM+ scene centered at 36.04°N, 97.87°W was acquired at 17 Universal Time Coordinates (UTC) on March 19, 2000, over the Oklahoma Southern Great Plains (SGP) Site of the U.S. Department of Energy's (DOE's) Atmospheric Radiation Measurement (ARM) Program during ARM Enhanced Shortwave Experiment (ARESE) II period (Figure 1). The solar zenith angle is

43 degrees. The cloud cover of the 185 km \times 180 km ETM+ scene is about 40 percent as shown in the gray scale image. The left portion of the scene is clear with a few small isolated cumuli. The right part of the image is covered with stratocumulus. Between the clear and the overcast are the scattered fair weather cumulus clouds and cloud streets. The cloud spacing gradually decreases as cloud cover increases from clear to overcast. Blowups of sub-images of 512 \times 512 pixels (15 km \times 15 km) from a completely clear region, and three consecutive cloudy images at the bottom show details of cloud structure (Figure 1).

During ARESE II, the Balloon-Borne Sounding System (BBSS) (Lesht 1995) was launched from the central facility every 3 hours to measure the vertical profile of the thermodynamic state of the atmosphere and wind speed. The Millimeter-Wavelength Cloud Radar (MMCR) (Clothiaux 2000) and

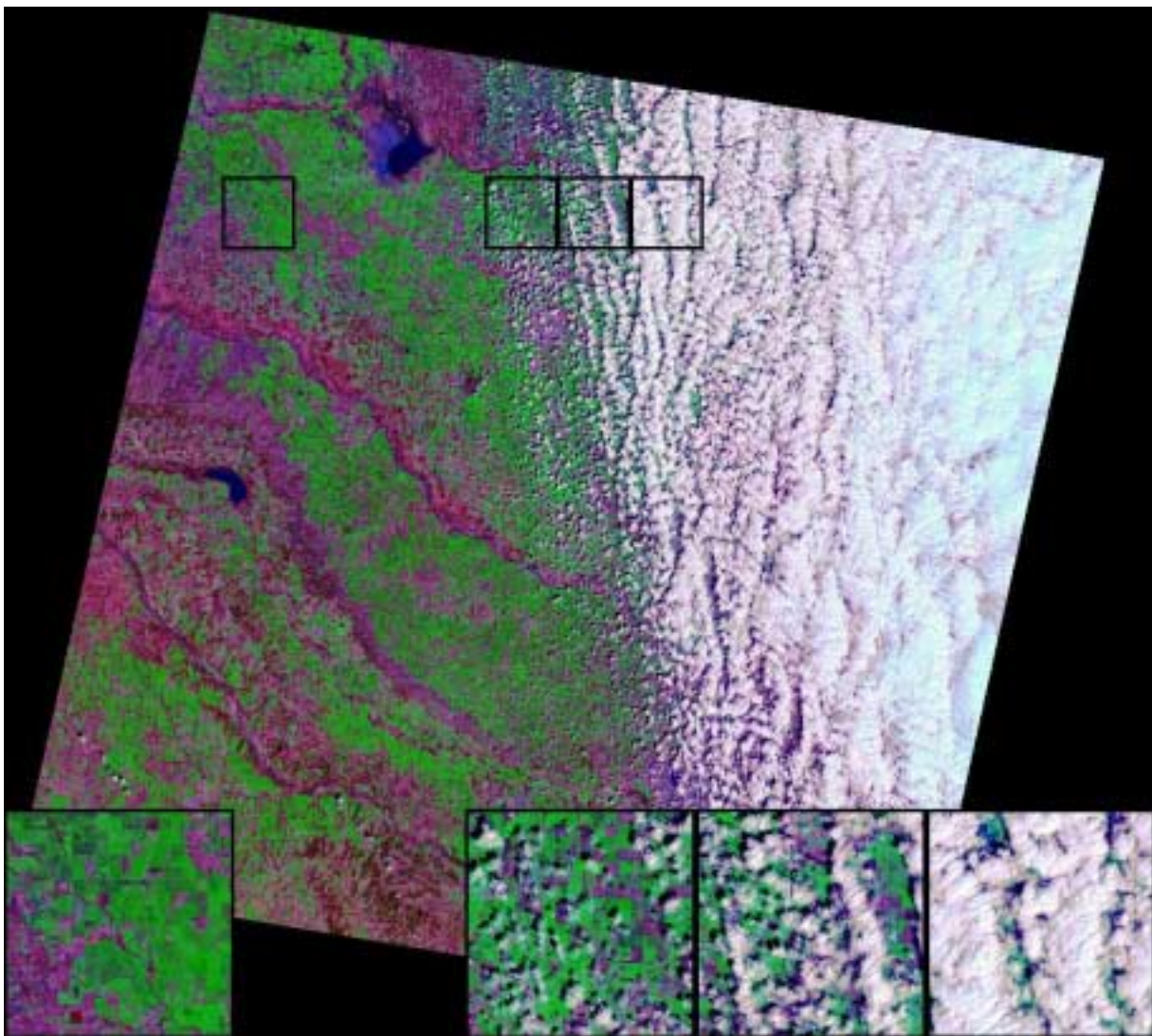


Figure 1. An ETM+ image acquired at 17 UTC on March 19, 2000, over the SGP ARM Site in Oklahoma. Blowup sub-images show details with a completely clear sub-image at left and three consecutive sub-images with increasing cloud cover toward the right.

Belfort Laser Ceilometer (BLC) (Turner 1996) located at the central facility site were operating continuously to measure cloud reflectivity and to detect the cloud base. The BBSS, MMCR, and BLC measurements show the cloud base at ~0.5 km and cloud top at ~1 km.

Data Analysis

Cumulus clouds can enhance the down-welling solar irradiance in the clear region nearby. In those clear regions, an enhancement of the reflected solar radiation is also expected. However, cumulus cloud fields are complex in nature (Cahalan and Joseph 1989, and Wielicki and Welch 1986). Other than the evident shadowing effects in high spatial resolution images, the effects of clouds on reflected sunlight in clear patches are not obvious. Even if the cloud effects can be identified, it may nevertheless be difficult to identify the major characteristics of cumulus clouds that cause these effects.

The major difficulty describing the effects of cumulus clouds comes from the fact that the surface reflectance subjects to large spatial and temporal variations. However, the surface reflectance in the visible (band 1 and 3) and the mid-IR (band 7) are highly correlated over vegetation, forest, and wet soil (Kaufman 1997). This information was used to determine the path radiance of clear atmosphere (Wen 1999). In the clear region of the cumulus cloud field, the visible and mid-IR correlation is still evident (Figure 2). The lower envelopes of the visible and mid-IR relations are shifted upwards. The intercept of straight line that fits though the lower envelope at zero of mid-IR no longer represents the path radiance of the atmosphere. This intercept is defined as apparent path radiance.

The apparent path radiance is evidently enhanced compared to the path radiance in the clear region. The enhancement of the apparent path radiance depends on the cloud spacing. Here, we used a mean cloud-free distance to characterize the cloud spacing. The shortest distance from a clear pixel to a cloud in the principal plane is defined as cloud-free distance for the clear pixel.

The apparent path radiance of sub-images of 512×512 pixels is plotted as a function of the mean cloud-free distance (Figure 3). The average of true path radiance from clear region is used as a reference. It is evident that the enhancement of the apparent path radiance increases as cloud-free distance decreases, exceeding 0.025 and 0.015 for band 1 and band 3, respectively, when the mean cloud-free distance is < 0.5 km. The enhancement decreases to an asymptotic value at a mean cloud-free distance about 2 km.

An analytical form of exponential decrease is used to parameterize the relationship. The nonlinear best fits for band 1 and 3 are

$$r_{0.49 \mu\text{m}} = 0.061e^{-\frac{x}{0.586}} + 0.090 \quad (1)$$

$$r_{0.66 \mu\text{m}} = 0.035e^{-\frac{x}{0.611}} + 0.027 \quad (2)$$

where x is the mean cloud-free distance in kilometers.

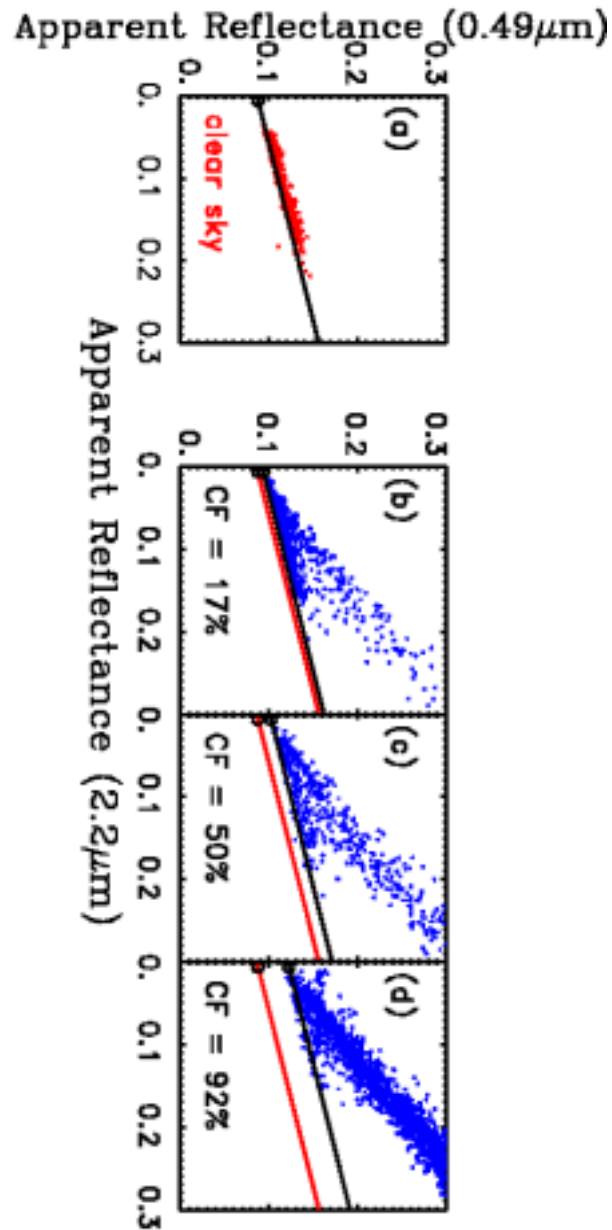


Figure 2. The relation between the visible at 0.49 μm (band 1) and the mid-IR band at 2.2 μm (band 7) for the four sub-images in Figure 1 (clear-sky at left, and three cloudy sub-images in the right with different cloud fraction indicated). The intercept of zero mid-IR reflectance of a straight line that fits through the lower envelope of the visible and mid-IR relations determines the path radiance (for completely clear-sky), and apparent path radiance (for clear patches in cumulus cloud field) respectively. The straight line used to determine the path radiance for clear-sky (left) is also plotted in cloudy cases as a reference (lower lines).

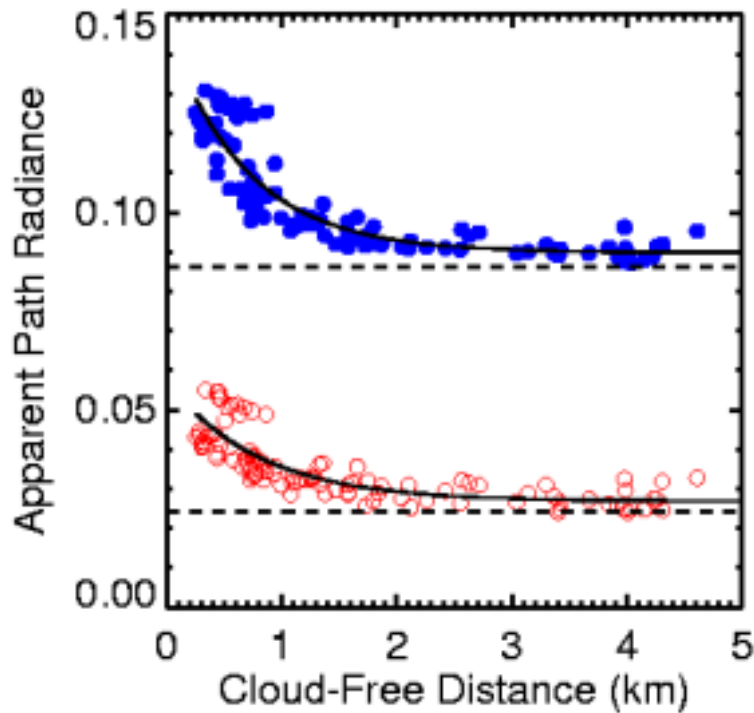


Figure 3. The apparent path radiance for ETM+ band 1 (solid circles) and band 3 (open circles) as a function of mean cloud-free distance, defined in the text.

Summary and Discussion

This study demonstrates the enhancement of upwelling sunlight observed using the high-resolution satellite imagery. Rather than examining each individual pixel, we introduced the apparent path radiance to characterize the enhancement. We found that the enhancement of apparent path radiance depends on mean cloud-free distance, and may be parameterized. The enhancement depends also on other factors (e.g., solar zenith angle, cloud thickness and height, and aerosol properties). Further research is necessary to fully understand the physical processes in clear-cloudy atmospheric conditions.

Acknowledgments

Data were obtained from the Atmospheric Radiation Measurement (ARM) Program sponsored by the U.S. Department of Energy, Office of Science, Office of Biological and Environmental Research, Environmental Sciences Division. This research was partly supported by the Department of Energy's ARM Program under Grant DE-A102-00ER62939.

Corresponding Author

G. Wen, wen@climate.gsfc.nasa.gov, (301) 614-6220

References

- Cahalan, R. F., and J. H. Joseph, 1989: Fractal Statistics of Cloud Fields. *Mon. Wea. Rev.*, **117**, 261-272.
- Clouthiaux, E. E., T. P. Ackerman, G. G. Mace, K. P. Moran, R. T. Marchand, M. A. Miller, and B. E. Martner, 2000: Objective determination of cloud heights and radar reflectivities using a combination of active remote sensor at the ARM CART sites. *J. Appl. Meteor.*, **39**, 645-665.
- Kaufman, Y. J., A. E. Wald, L. A. Remer, B. C. Gao, R. R., Li, and L. Flynn, 1997: The MODIS 2.1- μm channel correlation with visible reflectance for use in remote sensing of aerosol. *IEEE Trans. Geosci. Remote Sens.*, **35**, 1286-1298.
- Lesht, B. M., 1995: An evaluation of ARM radiosonde operational performance, *Proceeding of the Ninth Symposium on Meteorological Observations and Instrumentation*, American Meteorological Society, Boston, Massachusetts.
- Mims, F. M., and J. E. Frederick, 1994: Cumulus clouds and UV-B, *Nature*, **371**, 291.
- Turner, D. D., Comparisons of the micropulse lidar and the Belfort Laser Ceilometer at the Atmospheric Radiation Measurement Southern Great Plains Cloud and Radiation Testbed Site. In *Proceedings of the Sixth Atmospheric Radiation Measurement (ARM) Science Team Meeting*. U.S. Department of Energy, Washington, D.C. Available URL:
http://www.arm.gov/docs/documents/technical/conf_9603/turner_96.pdf
- Wen, G., S. C. Tsay, R. F. Cahalan, and L. Oreopoulos, 1999: Path radiance technique for retrieving aerosol optical thickness over land. *J. Geophys. Res.*, **104**, 31,321-31,332.
- Wielicki, B. A., and R. M. Welch, 1986: Cumulus cloud properties derived using Landsat satellite data. *J. Climate Appl. Meteor.*, **25**, 261-276.